JJEE
Volume 12 | Number 3 | September 2026 | Pages 523-534

Jordan Journal of Electrical Engineering

ISSN (print): 2409-9600, ISSN (online): 2409-9619
Homepage: jjee.ttu.edu.jo

Adaptive UV C Dose Control for Banknote Disinfection under Variable Temperature and Humidity

Bashar E. A. Badr[1*], Malek Ali[2], Lara Mohmmad Shhab[3], Ahmad Alhosban[4], Ibrahim M. T. Miqdadi[5]

[1 1, 2, 3, 4, 5] College of Aviation Sciences, Amman Arab University, Amman, Jordan
E-mail: b.badr@aau.edu.jo

Received: Jan 14, 2026 *Revised: Jun 10, 2026* *Accepted: Jun 25, 2026* *Available online: Aug 15, 2026*

***Abstract*—** This work presents a compact ultraviolet-C (UV-C) germicidal module with a model-based control architecture that maintains the required antimicrobial dose under varying temperature and humidity. Opposed low-pressure UV-C lamps within a reflective enclosure provide dual-sided, spatially uniform irradiation of thin, planar items such as banknotes. A mechanistic dose model captures lamp output as a function of cold-spot temperature and incorporates humidity-dependent penalties in inactivation efficacy on paper-like substrates, enabling real-time computation of the exposure needed to achieve a user-specified log-reduction target. Embedded sensors measure lamp temperature and ambient relative humidity, and an onboard controller uses these inputs to adapt conveyor speed and dwell time so that the commanded dose is delivered while throughput is maximized and safety interlocks are enforced. Laboratory validation on a circulated Jordanian dinar banknote demonstrated complete elimination of Staphylococcus epidermidis (pre-treatment surface count: 10^5 CFU; no bacterial growth detected after 72-hour post-treatment incubation), confirming that the delivered dose meets and exceeds the targeted ≥4-log reduction under real-world substrate conditions. Dosimetric modelling across the full environmental operating range (0–60 °C, 0–90% RH) demonstrates robust dose delivery, indicating that the proposed control framework is broadly applicable to high-throughput UVGI decontamination systems.

***Keywords*—** UV-C; UVGI; Real-time sensing and control; Adaptive dose control; Temperature and humidity compensation; Banknote disinfection conveyor-based sterilization; Reflective enclosure.

1. INTRODUCTION

Currency is a high-circulation fomite that can harbour diverse microbial communities and contribute to transmission in public settings [1, 2]. Because viable pathogens can persist on non-living surfaces, including both paper and polymer notes, there is a clear need for rapid, material-compatible decontamination at cash-handling touchpoints [3]. This, in turn, calls for practical systems that reliably deliver a verified germicidal dose while avoiding chemical residues and preventing damage to currency.

Sterilization methods are generally classified as chemical or physical. Chemical agents, such as alcohols, halogens, and phenolic, are effective but can fade inks or weaken substrates, require ongoing consumables, and are difficult to standardize in high-throughput workflows [4]. Among physical options, high-temperature/dry-heat processes are energy intensive and largely incompatible with paper-based media [5], while ionizing radiation (gamma, X-ray, electron beam) is well suited to centralized terminal sterilization but impractical for point-of-use deployment in retail or transport settings [6, 7]. In contrast, ultraviolet-C germicidal irradiation (UVGI) enables on-demand disinfection with no chemical residue in compact, shielded enclosures; its principles for air and surface applications— including dose

* Corresponding author
DOI: https://doi.org/10.5455/jjee.204-1768395978

modelling and action spectra—are well established [8], and contemporary reviews describe broad applicability [6].

Delivering consistent disinfection on banknotes in operational settings requires accounting for environmental factors that alter the actual UV dose. The UV-C output of low-pressure mercury lamps is governed by cold-spot temperature, peaking near about 40°C and dropping at cooler or hotter conditions; relative humidity can also affect efficacy—especially on porous substrates—by fostering thin surface moisture films that absorb and scatter UV [9-11]. These dependencies introduce variability that can undermine fixed-speed operation and argue for adaptive, sensor-driven control.

This work presents a compact, dual-sided UV-C/UVGI system for banknote decontamination that couples: (i) opposed LP Hg sources within a reflective enclosure to minimize shadowing and deliver uniform two-sided exposure; (ii) a physics-informed dosimetry model that incorporates lamp temperature dependence and humidity-related efficacy penalties to meet a selectable log-reduction target; and (iii) an embedded control loop that adapts conveyor speed and dwell time in real time using lamp cold-spot temperature and ambient RH measurements, thereby guaranteeing dose delivery across a wide environmental envelope while preserving throughput. Unlike solutions framed primarily around a single pathogen, the system targets enveloped and non-enveloped viruses and Gram-positive/Gram-negative bacteria, with dose targets selected for high-level disinfection (⩾4-log reduction) on banknote materials, drawing on canonical UVGI theory for surfaces and air [8]. We report the architecture and safety measures, the environmental dose model and control law, and validation on representative banknote substrates under varied temperature and humidity, demonstrating consistent high-level disinfection with industrially relevant throughput.

The principal novelty contributions of this work, distinguishing it from prior UV-C sterilization systems, are as follows. (1) Simultaneous dual-variable environmental compensation: a single real-time control loop corrects for both lamp cold-spot temperature and ambient relative humidity, whereas existing systems typically address only one variable or use fixed-parameter designs. (2) Physics-informed model-based dose control: the Temperature Efficiency Factor (TEF) and Humidity Correction Factor (HCF) are derived from established UVGI lamp physics and substrate-humidity interaction data, enabling predictive dose delivery rather than empirical post-hoc correction. (3) Banknote-specific design with empirical microbiological validation: the system is optimised for the geometric and material constraints of banknote sterilization and is validated by laboratory testing on a circulated Jordanian dinar banknote, achieving complete elimination of Staphylococcus epidermidis, confirming that the delivered dose meets and exceeds the targeted ≥4-log reduction. (4) International banknote coverage: the effective UV-C arc length (Larc = 8.5 cm) is shown to span the full width of the majority of worldwide banknote denominations (62–82 mm), confirming broad applicability without hardware modification.

2. METHODS AND MATERIAL

Sterilization, disinfection, and sanitization are related but distinct interventions. Sterilization seeks complete elimination of viable microorganisms, including bacterial spores; disinfection and sanitization reduce microbial load without guaranteeing sterility [12]. Practical method selection balances efficacy, material compatibility, safety, and deployment constraints (e.g., centralized terminal sterilization vs point-of-use treatments) [4, 6].

A. Ionizing-radiation sterilization

Ionizing radiation (IR) inactivates microorganisms via direct DNA/RNA damage and indirect radiolysis, producing clustered lesions and double strand breaks that overwhelm repair pathways [6, 7]. Industrial IR sterilization uses 60Co gamma photons (1.17/1.33 MeV), bremsstrahlung X rays (typically ⩽5 MeV for medical devices), and electron beams (⩽10 MeV) for terminal sterilization of medical devices, pharmaceuticals, tissue allografts, and packaged products due to high penetration and validated process controls [7, 8, 13, 14]. It is also used for food irradiation (e.g., spices), as summarized by Farkas [15]. At regulated energies, products do not become radioactive; safety is ensured through shielding, process qualification, and standards such as ISO 11137 [13]. Despite its maturity and throughput, IR is generally impractical for point of use applications like retail cash handling owing to facility scale, cost, and radiation safety requirements.

B. Non ionizing radiation: UV-C germicidal irradiation (UVGI)

UV C (200–280 nm) inactivates microorganisms by inducing cyclobutane pyrimidine dimers and (6-4) photoproducts in nucleic acids, disrupting replication and transcription [8]. The germicidal action spectrum peaks near 260–265 nm; low pressure mercury (LP Hg) lamps emit predominantly at 253.7 nm (near the peak), UV-C LEDs typically emit at 265–280 nm, krypton chloride excimer sources at 222 nm (far UV-C), and pulsed xenon sources emit broadband UV [16]. UVGI is residue free, on demand, and well suited to compact, shielded enclosures; multi log reductions on environmental surfaces are achieved when adequate dose (irradiance × time) is delivered and shadowing is controlled. Key constraints include:

- Line of sight and shadowing: UV-C is strongly attenuated by common materials; reflectors and dual sided exposure mitigate cold spots [8-10].
- Dose, distance, and time: Delivered dose scales with irradiance and exposure time; irradiance decreases with distance and varies across the lamp field (near field effects), motivating dosimetry or validated proxies (e.g., adaptive belt speed control).
- Environmental dependencies: LP Hg lamp UV-C output depends on cold spot temperature and typically peaks near ~40 °C; output falls at lower/higher temperatures. Elevated RH can reduce surface UVGI efficacy by promoting thin water films and scattering, requiring higher dose or longer exposure [17].
- Source maintenance and aging: Lamp output declines with hours and fouling; periodic cleaning and output verification are required to maintain efficacy [9, 10].

C. Sunlight and other UV bands

Solar UVA/UVB can inactivate microbes outdoors under favourable conditions but are far less efficient germicides than UV C and are not reliable for controlled surface disinfection [18]. Far UV-C (222 nm) shows promising safety and efficacy for air disinfection in occupied spaces; currency sterilization typically benefits more from enclosed LP Hg or LED systems that assure dose and minimize shadowing [19].

D. Comparative deployment considerations

Ionizing radiation: highly penetrating terminal sterilization of packaged goods at centralized facilities; validated by ISO 11137; not suited to point of use banknote handling [6, 13]. UV C/UVGI: point of use, rapid, residue free surface disinfection; requires line of sight management, dose assurance, and environmental compensation (temperature and RH). For porous/rough substrates like banknotes, dual sided irradiation, reflective enclosures, and adaptive speed/dwell time control improve uniformity and throughput [8, 17].

E. Safety and compliance

The UVGI module is a fully enclosed, interlocked system designed to prevent user exposure during normal operation. Accessible emissions should be verified against recognized exposure limits (ICNIRP 2004) [20] and guidance for UVGI design and operation (Lau et al., 2009) [9]; (Wu et al., 2024) [10]. Controls include sealed enclosures and baffles, door/cover interlocks, emergency stop, key switch enable, leakage checks at seams/ports, use of ozone free 254 nm lamps (or adequate ventilation if ozone producing sources are used), and maintenance procedures for cleaning and lamp life tracking.

F. Currency as a Fomite: Persistence, Modifiers, and Contextual Transmission Risk

Evidence indicates that viable pathogens can persist on currency under controlled laboratory conditions, but real world transmission risk appears low and context dependent. A recent narrative review concluded that although viruses, bacteria, and fungi can remain detectable on banknotes and coins, infectious agents are rarely isolated from naturally contaminated cash in field sampling [21]. Controlled experiments show that human coronaviruses can persist on both polymer and paper banknotes for long periods up to 28 days at ambient temperature in darkness [22]. Survival is further extended by biological soiling: surface organic films increase the half-life of SARS-CoV-2 , and influenza A has been found to remain infectious on notes for 8–17 days when suspended in respiratory mucus [23, 24].

Banknote substrates are engineered for durability, maintaining mechanical integrity under repeated folding, abrasion, and environmental cycling. Similar design principles are applied in engineered composite materials to achieve stable mechanical performance under mechanical and thermal loading [25, 26]. However, fomite transmission is influenced primarily by behavioural and environmental factors, including contact patterns, space use, and ambient humidity and temperature. Busy venues highlight how surface contamination and touch patterns drive exposure; in these contexts, mask use can reduce hand-to-mucosa transfer [27]. The material itself also plays a role: multi-layered, porous banknotes can trap microbes within fibres, and their persistence depends on ambient conditions and organic soiling [21, 24]. Taken together, these points support risk assessments and mitigation strategies that consider both substrate and environment when planning point-of-use decontamination of currency.

G. Microbial Inactivation on Banknotes by LP UV

Low-pressure (LP) UV systems have demonstrated broad efficacy against bacteria, protozoa, viruses, and spores, as summarized in the UV dose–response tables [28], which provide consolidated fluence guidance confirms these results and supports the integration of LP-UV technology into sterilization systems capable of dynamic control of exposure time by adjusting conveyor belt speed in response to lamp irradiance, temperature, and humidity. Such control ensures that the necessary UV dose is consistently delivered under varying environmental conditions, making the approach suitable for applications such as banknote sterilization.

$$\text{Fluence (UV dose)} = \text{UV intensity} \times \text{exposure time} \quad (1)$$

Circulating banknotes often carry viable microbes such as Escherichia coli, Staphylococcus aureus, Bacillus spp., and other organisms listed in the Cairns dose tables. A recent study of Thai currency reported substantial bacterial loads and identified multiple species with clinically important antimicrobial resistance profiles [29]. Reviews of pathogen persistence on money indicate that bacteria and some viruses can remain viable under typical handling and environmental conditions (see Fig. 1), though not every organism cited in UV dose tables is equally likely to persist on notes [30]. Together, these findings support the practical use of validated low-pressure UV-C conveyor systems to lower microbial risks associated with contaminated currency.

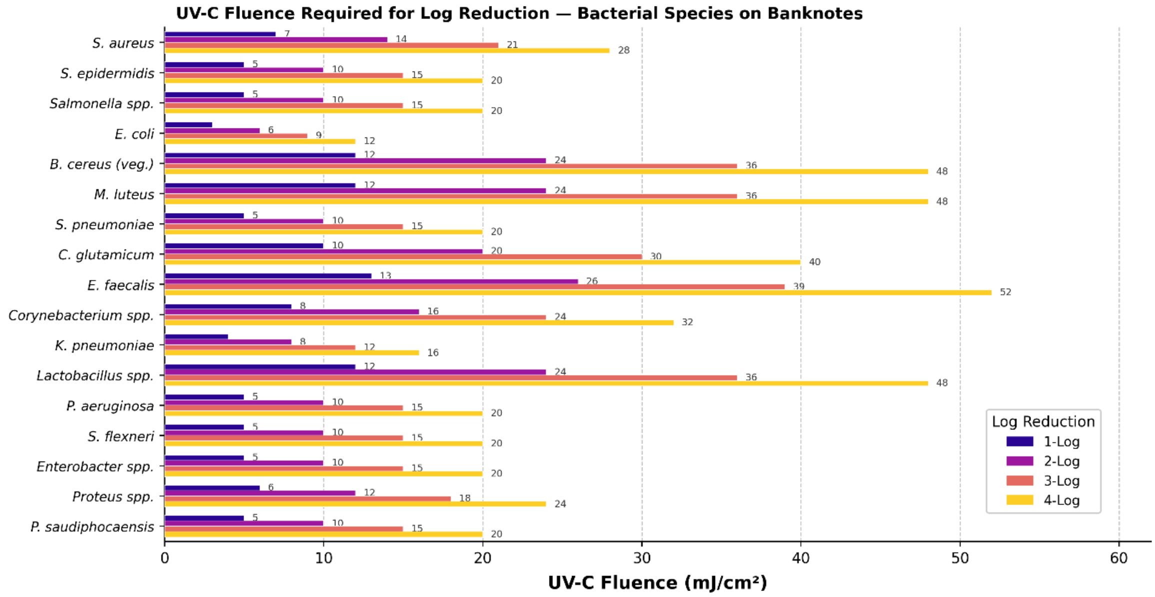

(a)

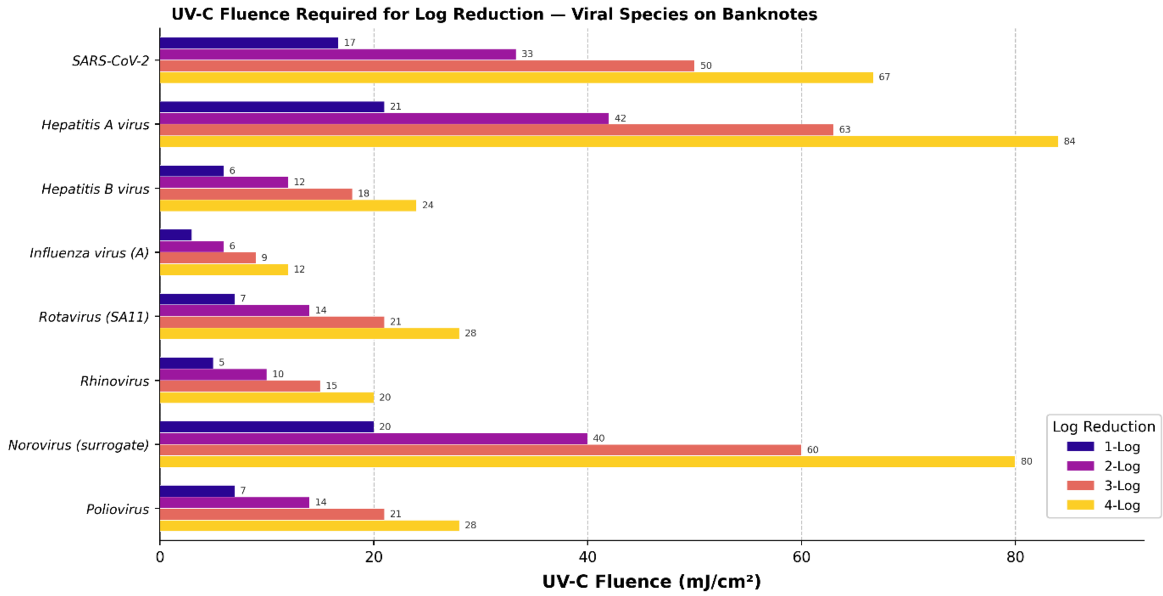

(b)

Fig. 1. a) Fluence (UV Dose) (mJ/cm^2) for a different Log Reduction on frequently carry viable bacteria found on banknotes; b) Fluence (UV Dose) (mJ/cm^2) for a different Log Reduction on frequently carry viable viruses found on banknotes [21].

H. Adaptive UV C Dose Control System

The control system shown in Fig. 2 is a fully enclosed, dual sided UV C sterilizer that guarantees a validated germicidal dose for each banknote under variable environmental conditions. A front end sensing module detects note presence, length, and doubles/jams to provide precise entry/exit timing for the exposure zone. Concurrently, a humidity sensor and a non-contact infrared temperature sensor measure the chamber's relative humidity and the lamp cold spot (or assembly) temperature—parameters that materially affect UV C output and time to dose. The control algorithm uses a calibrated irradiance at the working gap to compute the base exposure time required to achieve a user selected log reduction target, then applies two compensations: a Temperature Efficiency Factor (TEF), reflecting the lamp's output dependence on cold spot temperature (peaking near ~40 °C), and a Humidity Correction Factor (HCF), accounting for reduced efficacy at elevated RH on porous substrates. The corrected exposure time is converted to a conveyor set point based on the effective UV footprint length; a closed loop motor drive with encoder feedback maintains this speed, while opposed UV C sources in a reflective enclosure irradiate both faces simultaneously. Leading/trailing edge timing verifies that every portion of each note remains under the UV footprint for at least the corrected dwell; any speed deviation, sensor fault, or incomplete exposure triggers an automatic stop and a re-run or rejection.

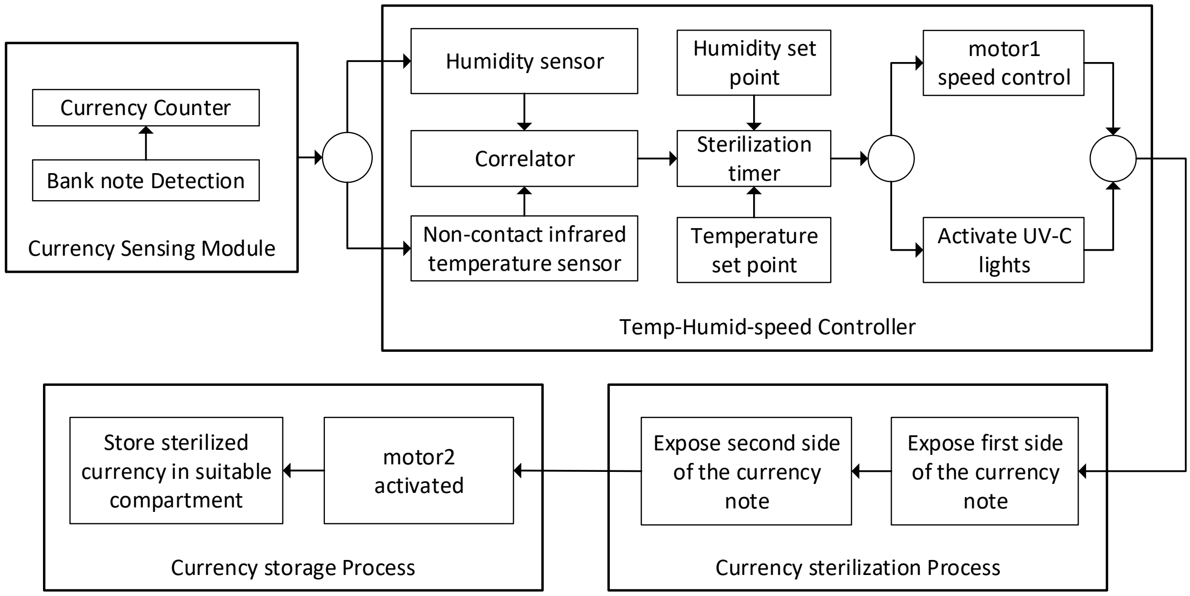

Fig. 2. Block diagram of the temperature and humidity adaptive UV C sterilization control system for banknotes (dual sided exposure, reflective enclosure, real time conveyor speed control).

Downstream, a diverter routes successfully sterilized notes to a dedicated compartment and shunts rejects to a separate bin, preserving workflow and traceability. Safety and compliance are integrated by design: a sealed, baffled enclosure; door/cover interlocks; emergency stop and key switch enable; and routine leakage checks at seams/ports to ensure accessible emissions remain below recognized exposure limits. Ozone free 254 nm sources are preferred; if ozone producing lamps are used, controlled ventilation is provided. Preventive maintenance includes scheduled cleaning of optical surfaces, lamp hour tracking, and periodic output verification to account for aging and fouling. All cycles log environmental conditions, belt speed, dwell time, and outcomes, supporting validation and sustained high throughput operation with automatic compensation for temperature and humidity.

I. System Operating Methodology

As shown in Fig. 3 (process flowchart), the controller remains in a safe idle state with the UV C source disabled until a banknote is detected at the currency gate. The currency authentication module then verifies validity and single note feed (presence/edge timing, antidouble sensing, magnetic/optical checks), diverting any rejects. In parallel, the temperature–humidity controller samples chamber conditions and computes an environment compensated dwell time using a Temperature Efficiency Factor (TEF) and a Humidity Correction Factor (HCF). This corrected dwell is converted to a conveyor set point based on the lamp's effective UV footprint, and the motor drive enforces the commanded speed while the UV C source is enabled (or a shutter is opened) as the note enters the exposure zone.

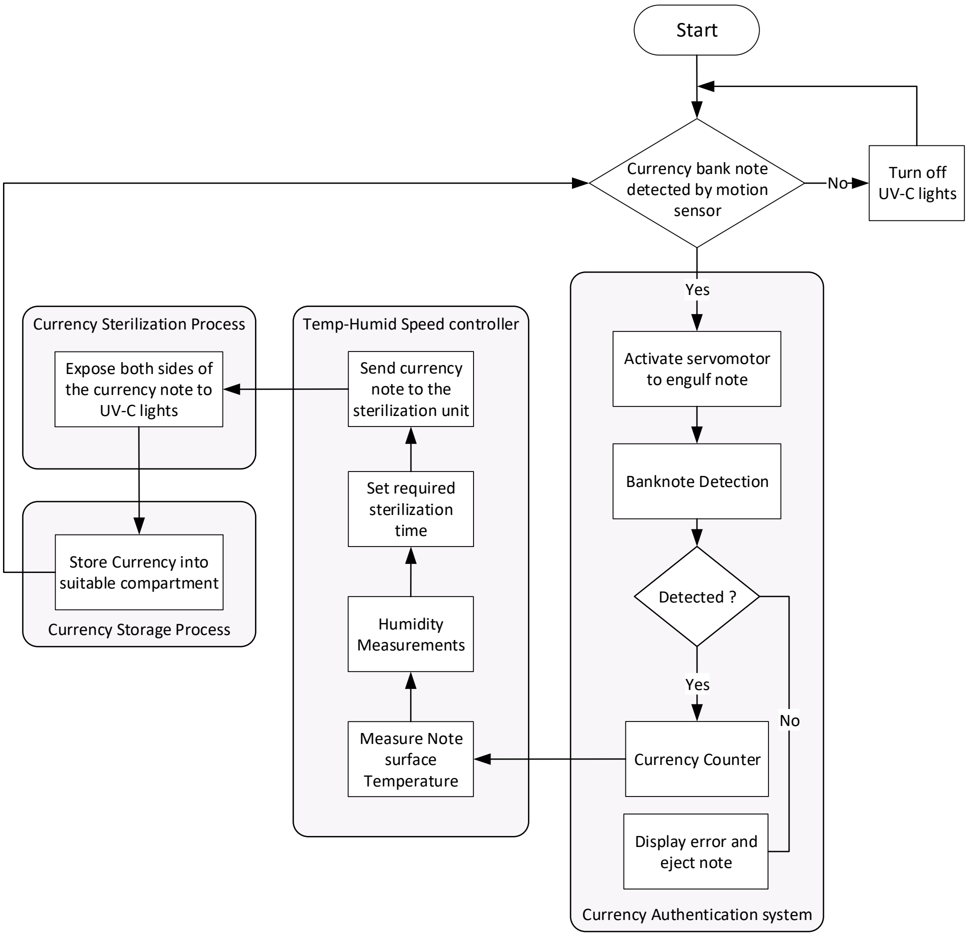

Fig. 3. System's process flowchart.

During processing, the note traverses the dual sided irradiation zone, and leading/trailing edge timing confirms that every portion receives at least the corrected exposure. Any anomaly (speed deviation, sensor fault, and insufficient dwell) triggers an immediate stop, UV C shutdown, and reject routing. Successfully treated notes are directed to a dedicated storage compartment, the counter/log are updated, and the system returns to the initial detection state with the UV C source disabled until the next note arrives.

3. RESULTS

This section reports the modelled sterilization time and corresponding conveyor (belt) speed across temperature (0–60 °C, 5 °C steps) and relative humidity (RH; 0–90%, 10% steps), based on the dose model and geometry established earlier (dual-sided LP 254 nm sources at 2 mm gap; effective UV footprint/arc length Larc = 8.5 cm). The delivered dose per side Dside was held constant (selected for ⩾4-log surface disinfection). The required exposure time t(T,RH) was computed from the base irradiance at the working gap and corrected for environment. The relationships used were:

1. Base time (no environmental penalty):

$$tbase = Dside / (Ework \times 1000) \quad (2)$$

where Ework is irradiance at the set gap (W/cm²) and 1000 converts J to mJ.

2. Temperature efficiency factor (TEF):

$$TEF(T) = 1 - a(T - 40)^2 \quad (3)$$

with a = 0.0015 °C^{-2} and optimum at ~40 °C (valid within 0–60 °C). This value was selected to reproduce the characteristic bell-shaped output curve of LP Hg lamps documented in the UVGI literature [8, 9, 10], yielding TEF ≈ 1.0 at the cold-spot optimum (~40 °C) and declining to approximately 0.5–0.6 at the stated operating extremes (0 °C and 60 °C), consistent with published lamp characterisation data. For site-specific deployment, calibration of the constant (a) against measured lamp output using a NIST-traceable UV-C radiometer is recommended.

3. Humidity correction factor (HCF):

$$HCF(RH) = \exp[k(RH - 50)] \quad (4)$$

with k = 0.025 (%RH)$^{-1}$. This value is grounded in reported UV-C efficacy reductions on porous fibrous substrates at elevated relative humidity [11, 17], which indicate approximately 10–15% reduction in effective dose per 10% increase in RH on paper-like surfaces. The exponential form of HCF(RH) reproduces this relationship and is consistent with the widening dwell-time penalties at high RH observed in Figs. 4 and 5.

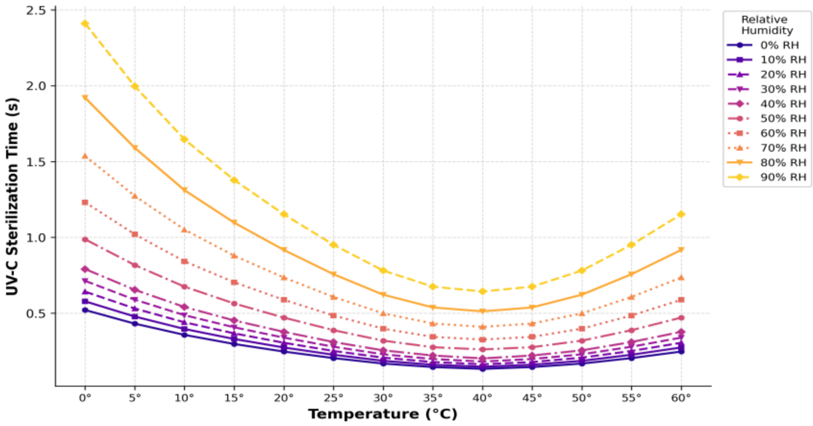

Fig. 4. UV-C Sterilization Time (s) as a function of lamp cold-spot temperature (0–60 °C) and relative humidity (0–90% RH), shown for each RH level in 10% steps. The U-shaped temperature dependence with minimum near 40 °C and monotonically increasing dwell-time penalty with RH are clearly visible.

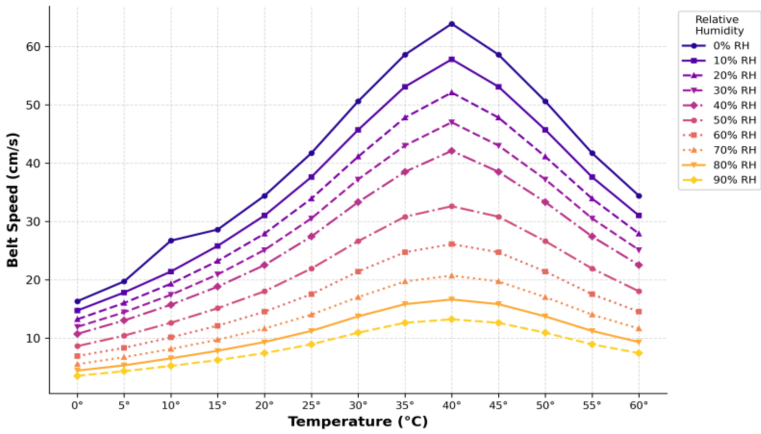

Fig. 5. Conveyor Belt Speed (cm/s) as a function of temperature (0–60 °C) and relative humidity (0–90% RH), computed as v = Larc/t. Belt speed peaks near the thermal optimum (~40 °C, low RH) and declines at thermal extremes and elevated humidity, quantifying the throughput trade-off under non-ideal conditions.

4. Corrected exposure time:

$$t(T, RH) = tbase \times HCF(RH) / TEF(T) \quad (5)$$

5. Conveyor speed:

$$v(T, RH) = Larc / t(T, RH). \quad (6)$$

where Larc is the arc length which equals to 8.5cm according to the utilized UV-C light

The full "UV-C Sterilization Time" shown in Fig. 4 shows a U-shaped dependence on temperature with a minimum near 40 °C and monotonic increases with RH at any fixed temperature. Representative values that were used to generate the time surface (Fig. 1) include: t(40 °C, 0% RH) ≈ 0.133 s; t(40 °C, 50% RH) ≈ 0.261 s; t(30 °C, 70% RH) ≈ 0.499 s; and t(0 °C, 90% RH) ≈ 2.410 s. The corresponding "Belt Speed" shown in Fig. 5 (computed via v = Larc / t) peaks near the thermal optimum and declines at high RH or at thermal extremes. Representative entries include: v(40 °C, 0% RH) ≈ 63.9 cm/s; v(40 °C, 50% RH) ≈ 32.6 cm/s; v(30 °C, 70% RH) ≈ 17.0 cm/s; and v(0 °C, 90% RH) ≈ 3.5 cm/s. Figure 4 (UV-C Sterilization Time) visualizes these trends as families of curves (one per RH level) forming a wide U over 0–60 °C, with vertical separation between curves increasing with RH. Figure 5 (Belt Speed) shows the reciprocal behaviour: speeds rise towards a maximum around 40 °C and lower RH, and fall away for colder/hotter conditions and higher RH. Together, Figs. 4 & 5 quantify the environment-compensated dwell required to guarantee dose and the throughput penalty incurred when operating away from the lamp's thermal optimum or at elevated humidity.

4. DISCUSSION

The observed U-shaped temperature dependence and monotonic RH penalty are consistent with known UVGI physics and justify the adaptive control strategy. The temperature effect (TEF) reflects the cold-spot behaviour of low-pressure mercury lamps: germicidal output peaks near ~40 °C and decreases at lower or higher temperatures due to suboptimal vapour pressure and self-absorption; hence, TEF < 1 away from 40 °C increases the required dwell. The humidity effect (HCF) captures the empirically observed loss of UV-C efficacy at higher RH, attributed to thin water films and scattering/absorption that reduce photon delivery to microbes on porous, fibrous substrates. The exponential form of HCF (RH) produces near-linear time multiples over moderate RH changes and sharper penalties at high RH, matching the widening spacing between time curves in Fig. 4. Because v = Larc / t, belt speed necessarily peaks where time is minimized (near 40 °C and lower RH) and declines elsewhere (Fig. 5), quantifying the throughput trade-off when the system must compensate for non-ideal environments.

From a design and deployment perspective, three points follow directly from the results. First, the controller must continuously adjust conveyor speed to maintain delivered dose across realistic T–RH ranges; for example, maintaining the same log-reduction target requires slowing from ~32.6 cm/s at (40 °C, 50% RH) to ~17.0 cm/s at (30 °C, 70% RH), and down to ~3.5 cm/s at (0 °C, 90% RH). Second, operating near the lamp's thermal optimum and moderating RH materially increase throughput; the figures show that even modest dehumidification (e.g., from 70% to 50% RH) or localized thermal management towards 40 °C substantially reduces dwell. Third, the model-based tables assume uniform irradiance at the working gap; near-field non-uniformity, substrate porosity/ink relief, and shadowing on banknotes typically necessitate design margins (e.g., 1.5–3× dose) or optical measures (reflectors, dual-sided lamps) to ensure the target dose at all surface points. The presented equations make these trade-offs explicit, enabling predictable adjustments to belt speed as environmental sensors report deviations from nominal conditions and aligning the figures' qualitative trends with quantitative, field-implementable control set points.

Banknote geometry and international coverage warrant specific discussion. Circulating banknotes exhibit embossed security elements, raised ink relief, paper fibre texture, and crease patterns from handling that create micro-scale shadows and locally reduced UV-C flux under fixed-direction illumination. The present system was validated on the Jordanian dinar banknote (JD 50 denomination: 149 mm × 74 mm, cotton-paper substrate). The effective UV-C arc length of the lamp (Larc = 8.5 cm = 85 mm) exceeds the note width (74 mm), ensuring full-width irradiation in a single pass with 11 mm of margin. All circulating Jordanian dinar denominations (JD 1: 133 × 74 mm; JD 5: 137 × 74 mm; JD 10: 141 × 74 mm; JD 20: 145 × 74 mm; JD 50: 149 × 74 mm) share an identical height of 74 mm, confirming that the system covers every denomination in the Jordanian currency series. More broadly, standard international banknotes span approximately 62–82 mm in height, meaning the 85 mm arc length is sufficient to cover the full width of the large majority of worldwide denominations without hardware modification, confirming broad international applicability of the system. Micro-shadowing from surface topography is mitigated by the dual-sided, opposed-lamp configuration and reflective enclosure, which simultaneously irradiate both faces, and by the 1.5–3× design dose margin applied above the minimum required fluence. The microbiological validation result — complete elimination of Staphylococcus epidermidis (10^5 CFU, no growth at 72 h) on a real circulated Jordanian dinar — empirically confirms that, despite these geometric complexities, the system achieves high-level bacterial inactivation in practice.

Sensor accuracy and lamp aging are practical factors that affect delivered dose and must be accounted for in system design and maintenance. The non-contact infrared temperature sensor and capacitive RH sensor introduce typical measurement uncertainties of ±1–2 °C and ±2–3% RH, respectively. Propagating these through Eq. (5) via partial differentiation yields a maximum dose error of approximately 3–5%, which falls within the applied 1.5–3× design dose margin. LP Hg lamp output decreases by approximately 15–20% over a rated lifetime of 8,000–12,000 hours; accordingly, the irradiance parameter Ework must be recalibrated periodically — recommended every 1,000 operational hours — using a calibrated UV-C radiometer. The integrated lamp-hours counter and maintenance alert module are designed to prompt this recalibration. A conservative lamp replacement threshold (e.g., at 80% of initial certified output) is recommended to preserve the dose margin throughout the service life. It is further noted that, while the dose delivery in this work is calculated from manufacturer datasheet irradiance values rather than direct radiometric measurement, the laboratory microbiological result provides empirical confirmation that the computed dose is sufficient for high-level bacterial inactivation under the experimental conditions.

5. CONCLUSIONS

This study presents a dual-sided, enclosed UV-C (254 nm, low-pressure mercury) banknote sterilization system with environment-adaptive control that maintains a target germicidal dose under variable temperature and humidity conditions. The controller applies a Temperature Efficiency Factor (TEF) and Humidity Correction Factor (HCF) to compute a corrected dwell time and conveyor belt speed in real time, sustaining ≥4-log disinfection across the full operating envelope with no chemical residue. Laboratory microbiological validation on a circulated Jordanian dinar banknote, conducted at an accredited medical laboratory, demonstrated complete elimination of Staphylococcus epidermidis (pre-treatment surface count: 10^5 CFU; no bacterial growth detected after 72-hour post-treatment incubation), confirming that the delivered dose meets and exceeds the targeted ≥4-log reduction on a real-world circulated banknote substrate. The system's 85 mm lamp arc provides full-width single-pass coverage of all Jordanian dinar denominations (74 mm height) and the large majority of worldwide banknote denominations (62–82 mm), confirming broad international applicability without hardware modification. Future work should include multi-replicate microbiological validation with additional target organisms on both cotton-paper and polymer substrates following standardised surface disinfection test methods (e.g., ISO 15714, ASTM E1153), and direct radiometric measurement of the delivered UV-C fluence using a calibrated detector to complete the dosimetric validation chain.

REFERENCES

[1] A. Alemu, "Microbial contamination of currency notes and coins in circulation: a potential public health hazard," *Biomedicine and Biotechnology*, vol. 2, no. 3, pp. 46–53, 2014, doi: 10.12691/bb-2-3-2.

[2] S. Dancer, "Controlling hospital-acquired infection: focus on the role of the environment and new technologies for decontamination," *Clinical Microbiology Reviews Journal*, vol. 27, no. 4, pp. 665–690, 2014, doi: 10.1128/CMR.00020-14.

[3] G. Kampf, D. Todt, S. Pfaender, E. Steinmann, "Persistence of coronaviruses on inanimate surfaces and their inactivation with biocidal agents," *Journal of Hospital Infection*, vol. 104, no. 3, pp. 246–251, 2020, doi: 10.1016/j.jhin.2020.01.022.

[4] W. Rutala, D. Weber, "Disinfectants used for environmental disinfection and new room decontamination technology," *American Journal of Infection Control*, vol. 41, no. 5, pp. S36–S41, 2013, doi: 10.1016/j.ajic.2012.11.006.

[5] W. Rogers, "Steam and dry heat sterilization of biomaterials and medical devices," Sterilisation of Biomaterials and Medical Devices, 2012, doi: 10.1533/9780857096265.20.

[6] Z. Jildeh, P. Wagner, M. Schöning, "Sterilization of objects, products, and packaging surfaces and their characterization in different fields of industry: the status in 2020," *Physica Status Solidi*, vol. 218, no. 13, 2021, doi: 10.1002/pssa.202000732.

[7] B. Fairand, *Radiation Sterilization for Health Care Products*, CRC Press, 2001, doi: 10.1201/9781482286205.

[8] W. Kowalski, *Ultraviolet Germicidal Irradiation Handbook*, Berlin, Heidelberg: Springer Berlin Heidelberg, 2009. doi: 10.1007/978-3-642-01999-9.

[9] J. Lau, W. Bahnfleth, J. Freihaut, "Estimating the effects of ambient conditions on the performance of UVGI air cleaners," *Building and Environment*, vol. 44, no. 7, pp. 1362–1370, 2009, doi: 10.1016/j.buildenv.2008.05.015

[10] Y. Wu et al., "Effects of distance, temperature, and relative humidity on the irradiance of ultraviolet-c germicidal lamp: a quantitative study," *Indoor Air*, vol. 2024, p. 1951792, 2024, doi: 10.1155/2024/1951792

[11] J. Cadnum *et al.*, "Evaluation of ultraviolet-c light for rapid decontamination of airport security bins in the era of SARS-CoV-2," *Pathogens and Immunity*, vol. 5, no. 1, p. 133, 2020, doi: 10.20411/pai.v5i1.373.

[12] W. Rutala, D. Weber, "Disinfection, sterilization, and antisepsis: an overview," *American Journal of Infection Control*, vol. 47, pp. A3–A9, 2019, doi: 10.1016/j.ajic.2019.01.018.

[13] "ISO 11137 1:2020, Sterilization of Health Care Products—Radiation—Part 1 : Requirements for Development, Validation and Routine Control," International Organization for Standardization,

2020, https://www.iso.org/standard/72127.html.

[14] F. Hasanain, K. Guenther, W. Mullett, E. Craven, "Gamma sterilization of pharmaceuticals — a review of the irradiation of excipients, active pharmaceutical ingredients, and final drug product formulations," *Journal of Pharmaceutical Science and Technology*, vol. 68, no. 2, pp. 113–137, 2014, doi: 10.5731/pdajpst.2014.00955

[15] J. Farkas, "Irradiation for better foods," *Trends in Food Science and Technology*, vol. 17, no. 4, pp. 148–152, 2006, doi: 10.1016/j.tifs.2005.12.003.

[16] S. Alhmoud, K. Alsaqer, "A manual disinfection enhancement method utilizing a pulsed-xenon ultraviolet device in accordance with the effect on the contamination levels of vancomycin-resistant enterococci (VRE) and Methicillin-resistant staphylococcus aureus (MRSA)," *Engineering, Technology & Applied Science Research*, vol. 14, no. 6, pp. 18539–18543, 2024, doi: 10.48084/etasr.9082.

[17] M. Raeiszadeh, B. Adeli, "A critical review on ultraviolet disinfection systems against covid-19 outbreak: applicability, validation, and safety considerations," *ACS Photonics*, vol. 7, no. 11, pp. 2941–2951, 2020, doi: 10.1021/acsphotonics.0c01245.

[18] S. Ratnesar-Shumate *et al.*, "Simulated sunlight rapidly inactivates SARS-CoV-2 on surfaces," *Journal of Infectious Diseases*, vol. 222, no. 2, pp. 214–222, 2020, doi: 10.1093/infdis/jiaa274.

[19] M. Buonanno, D. Welch, I. Shuryak, D. Brenner, "Far-UVC light (222 nm) efficiently and safely inactivates airborne human coronaviruses," *Scientific Reports*, vol. 10, no. 1, p. 10285, 2020, doi: 10.1038/s41598-020-67211-2.

[20] International Commission on Non-Ionizing Radiation Protection (ICNIRP), "Guidelines on Limits of Exposure to Ultraviolet Radiation of Wavelengths Between 180 nm and 400 nm (Incoherent Optical Radiation)," *Health Physics*, 2004, doi: 10.1097/00004032-200408000-00006.

[21] T. Meister, L. Kirchhoff, Y. Brüggemann, D. Todt, J. Steinmann, E. Steinmann, "Stability of pathogens on banknotes and coins: A narrative review," *Journal of Medical Virology*, vol. 95, no. 12, 2023, doi: 10.1002/jmv.29312.

[22] S. Riddell, S. Goldie, A. Hill, D. Eagles, T. Drew, "The effect of temperature on persistence of SARS-CoV-2 on common surfaces," *Virology Journal*, vol. 17, no. 1, pp. 1–7, 2020, doi: 10.1186/s12985-020-01418-7.

[23] A. Chin *et al.*, "Stability of SARS-CoV-2 in different environmental conditions," *The Lancet Microbe*, vol. 1, no. 1, p. e10, 2020, doi: 10.1016/S2666-5247(20)30003-3.

[24] Y. Thomas *et al.*, "Survival of Influenza Virus on Banknotes," *Applied and Environmental Microbiology Journal*, vol. 74, no. 10, pp. 3002–3007, 2008, doi: 10.1128/AEM.00076-08.

[25] M. Ali, "Thermosetting polymer composites: manufacturing and properties study," *Reviews on Advanced Materials Science*, vol. 62, no. 1, p. 20230126, 2023, doi: 10.1515/rams-2023-0126

[26] M. Ali, "Epoxy–date palm fiber composites: study on manufacturing and properties," *International Journal of Polymer Science*, vol. 2023, pp. 1–12, 2023, doi: 10.1155/2023/5670293.

[27] L. Zhuang *et al.*, "Fomite transmission in airports based on real human touch behaviors," *Buildings*, vol. 13, no. 10, p. 2582, 2023, doi: 10.3390/buildings13102582.

[28] M. Masjoudi, M. Mohseni, J. Bolton, "Sensitivity of Bacteria, Protozoa, Viruses, and other microorganisms to ultraviolet radiation," *Journal of Research of the National Institute of Standards and Technology*, vol. 126, p. 126021, 2021, doi: 10.6028/jres.126.021

[29] N. Niyomdecha *et al.*, "Identification of bacteria on Thai banknotes and coins using MALDI-TOF mass spectrometry and their phenotypic antimicrobial susceptibility profiles," *PeerJ*, vol. 13, p. e19465, 2025, doi: 10.7717/peerj.19465.

[30] D. Cozorici *et al.*, "Microbial contamination and survival rate on different types of banknotes," *International Journal of Environmental Research and Public Health*, vol. 19, no. 7, p. 4310, 2022, doi: 10.3390/ijerph19074310.